Seeing through Bone with Surface-Enhanced Spatially Offset Raman Spectroscopy

Bhavya Sharma,[†] Ke Ma,[‡] Matthew R. Glucksberg,[‡] and Richard P. Van Duyne[*,†,‡]

[†]Department of Chemistry and [‡]Deptartment of Biomedical Engineering, Northwestern University, 2145 Sheridan Road, Evanston, Illinois 60208-3113, United States

S *Supporting Information*

ABSTRACT: Surface-enhanced spatially offset Raman spectroscopy (SESORS) is a label-free vibrational spectroscopy that has the potential for *in vivo* imaging. Previous SESORS experiments have been limited to acquiring spectra using SERS substrates implanted under the skin or from nanoparticles embedded in tissue. Here we present SESORS measurements of SERS active nanoparticles coated with a Raman reporter molecule (nanotags) acquired, for the first time, through bone. We demonstrate the ability of SESORS to measure spectra through various thicknesses (3−8 mm) of bone. We also show that diluted nanotag samples ($\sim 2 \times 10^{12}$ particles) can be detected through the bone. We apply a least-squares support vector machine analysis to demonstrate quantitative detection. It is anticipated that these through-bone SESORS measurements will enable real-time, non-invasive spectroscopic measurement of neurochemicals through the skull, as well as other biomedical applications.

Imaging of the brain is generally performed using techniques such as magnetic resonance imaging (MRI), functional MRI (fMRI), computed axial tomography (CT), and positron emission tomography (PET).[1,2] These techniques allow for imaging of various brain functions, including blood flow, glucose uptake, and oxygen consumption,[2] which are usually reported as a ratio of change with respect to the brain at rest. Although these modalities are useful, they do have some limitations in terms of brain imaging. PET is the only technique which provides a reliable, quantitative measure of blood flow and oxygen consumption because it has been validated against standards, but it requires use of radioactive isotopes. fMRI does not have an absolute reference standard to which it can be compared and relies on the blood oxygen level dependent (BOLD) signal, which correlates with deoxyhemoglobin levels that can fluctuate due to changes in blood volume or oxygenation.[1,2] CT is an X-ray-based technology which has very good resolution and can be used to detect structural changes, but it does not provide any functional information.[1] Additionally, these techniques do not allow for quantification of neurotransmitters present in the brain.

Neurotransmitters such as dopamine and serotonin play critical roles in neurological functions, however little is known about their local concentrations in the brain. Normally the concentrations of these neurotransmitters are measured exogenously, either in the blood or urine, where the concentrations are significantly lower than in the brain. The only local concentration measures have been achieved using fast scan cyclic voltammetry, where holes are drilled in the skull, electrodes are inserted into parts of the brain known to release dopamine, and local measurements of dopamine are made.[3−6] Wightman et al., found the local concentrations to be on the order of 1−3 μM.[6] To more fully understand brain function, a non-invasive methodology for measuring concentrations of key neurochemicals needs to be developed.

With optical imaging, the brain can be studied *in vivo*, using near-infrared (NIR) light for penetrating the skin, skull, and brain.[1] There are a variety of endogenous and exogenous forms of contrast that provide information about the structure and function of tissues over a large scale from single cells to whole organism imaging.[7] The different absorptive properties of cell components, and intrinsic fluorescence from proteins, lipids, and metabolites, can all be used as forms of contrast for imaging.[7] Techniques for optical imaging include optogenetics,[8] two-photon microscopy,[9] and optical coherence tomography (OCT).[10] With these techniques, *in vivo* studies can be performed over multiple time points and in a non-destructive manner, however these techniques are all invasive. Optogenetics and OCT both involve drilling holes in the skull to insert optrodes and catheters, respectively; in two photon microscopy, a craniotomy must be performed to gain access to brain. Additinally, for all of these techniques, there is a trade-off between imaging depth and resolution.[7]

Here, we present a non-invasive method for spectroscopic measurements of tissue through bone. Our approach utilizes the combined power of two Raman spectroscopies, surface-enhanced Raman spectroscopy (SERS) and spatially offset Raman spectroscopy (SORS). SERS is a powerful vibrational spectroscopy that allows for label-free, highly sensitive and selective detection of low concentration analytes through amplification of the localized plasmon resonances of small noble metal nanoparticles. Although SERS began as an electrochemical method more than 35 years ago,[11] it has been applied in many areas of research, including biology, in recent decades.[12−14] Many of the biological applications of SERS have been performed *in vitro*, with cells, bacteria, and in various tissues.[15−17]

SORS allows Raman measurements to be made through distinctly different layers within a diffusely scattering medium.[18−21] In SORS, the Raman spectra are collected

from a location that is spatially offset from the incident laser beam. In this experiment, the photons that scatter from the surface of the bone return to the collection optics on the same trajectory as the incident beam. Photons that interact with the tissue behind the bone diffuse laterally in the material and are scattered in a wide angular distribution around the incident laser excitation at the surface. This allows for sub-surface spectra to be preferentially collected. Additionally, SORS can suppress auto-fluorescence arising from the surface.[21] By combining SERS and SORS, it has been demonstrated that SORS measurements can be made at greater depths than previously possible,[22,23] and has made *in vivo* applications of SERS possible. This combined surface-enhanced SORS is designated as SESORS. We have previously demonstrated the use of SESORS for *in vivo* glucose sensing.[24,25]

We demonstrate here the first SESORS measurements of nanoparticles embedded in tissue through bone. Previous studies have demonstrated that with strongly enhancing nanoparticles, such as SERS nanotags which are known to have enhancement factors of up to 10^8,[26,27] it is possible to measure SERS signals to depths of 20−25 mm in tissue.[22,23] Our approach involved injecting nanotags, ∼90 nm gold cores with a Raman reporter molecule *trans*-1,2-bis(4-pyridyl)-ethylene (BPE) on the surface, encased in ∼50 nm silica shells (Cabot Security Materials Inc., Mountain View, CA), into ovine tissue attached to a bone. Using previously described instrumentation[25] we collected SESORS spectra through the bone. Briefly, spectra were collected at 785 nm laser excitation using collection optics and a custom-made 26 fiber bundle, with the fibers arranged in a 6 mm diameter circle on the collection end, and vertically aligned at the detection end (Figure 1a). The nanotags were injected (volume = 100 μL, which

corresponds to a maximum dosing of ∼9×10^{13} particles) into the tissue adjacent to the bone, and with the laser incident on the bone surface, SESORS spectra were collected through the bone (Figure 1b). The bolus of nanotags expanded in the tissue when injected, so we believe the actual number of particles contributing to the SESORS signal is less than the total number of particles given above. Quantification of the number of particles contributing to the SESORS signal is currently under way.

Studies on the optical properties of the skull measured the absorption and scattering coefficients at wavelengths of 650 to 950 nm[1,28] and 800−2000 nm.[29] These studies found that cranial bones are partially transparent at 785 nm, allowing the NIR light to penetrate the skull. Post-mortem forensic measurements of skull bones have determined that the thickness of the human skull depends on both location of bone on skull and gender of person, with thicknesses ranging from 3 to 14 mm and an average thickness of 8 mm.[30] To test the feasibility of applying our methodology to studying the brain, we collected SESORS spectra through various thicknesses of the ovine bone, ranging from 3 to 8 mm thick.

Spectra were acquired at different locations along the bone, with thickness increasing from 3 to 8 mm, with 1 mm increments. The uncorrected spectra show residual fluorescence from the bone, as well as a peak at 960 cm^{-1}, which arises from the bone phosphate ν_1 mode[31] (Figure S1). The raw spectra were processed by baseline fitting and subtraction. These baseline-corrected spectra were plotted in a waterfall plot (Figure 2A), where it is evident that the BPE signal intensity decreases with increasing bone thickness. The representative SESORS spectra (Figure 2B) show how the thickness of bone affects the SESORS intensity. We note that even at 8 mm bone thickness, the characteristic peaks of BPE are still observable. Specifically, the A_{1g} modes of BPE at 1008 (ν_{13}), 1200 ($\nu_{9,10}$), 1338 (ν_6), 1604 (ν_2), and 1640 (ν_1) cm^{-1} are clearly visible.[26,32] The efficiency of scattering detection through the bone was determined by comparing the integrated intensity of the 1200 cm^{-1} peak through the various thicknesses of bone to the integrated integrated intensity of the same peak from spectra collected through a cuvette. The scattering efficiencies were calculated as the integrated intensity of the BPE peak from the through the bone spectra normalized by the accumulation time and laser power divided by the same value for the BPE nanotags in a cuvette. The values range from 3.5% at 3 mm down to 0.2% at 8 mm. These results indicate that a large amount of the Raman scattered signal is lost in traveling through the bone. However, even with 0.2% scattering efficiency, the spectra are strong enough to be seen with the eye.

In addition to determining the thickness of bone through which the SESORS data could be collected, we also investigated the concentration of BPE nanotags required to obtain a signal. SESORS spectra were taken of the original BPE nanotags sample, along with 10×, 20×, 30×, 35×, and 40× dilutions, utilizing the same piece of bone. We removed the original tissue and used fresh samples of tissue behind the bone to collect spectra. A volume of 100 μL of nanotags was injected into each piece of tissue, and spectra were collected at the 3 mm bone thickness. We found that we were able to obtain SESOR spectra even down to the 40× dilution (∼2×10^{12} particles).

We also performed chemometric analysis for quantitative detection utilizing the least-squares support vector machine regression (LS-SVR) method and leave-one-out (LOO) cross-
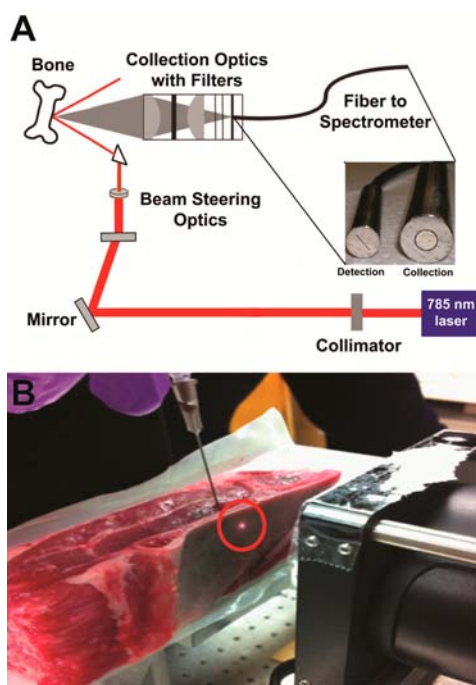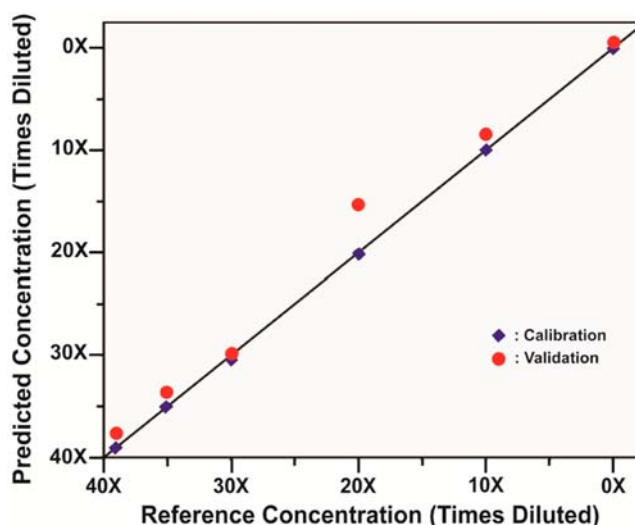

Figure 1. (A) Schematic of SESORS instrumentation, with collection and detection ends of fiber shown. (B) 785 nm laser spot (circled in red) on ovine shoulder bone with tissue attached. The BPE nanotags were injected into the tissue at several locations adjacent to the bone and SESORS spectra were collected through the different thicknesses of bone.
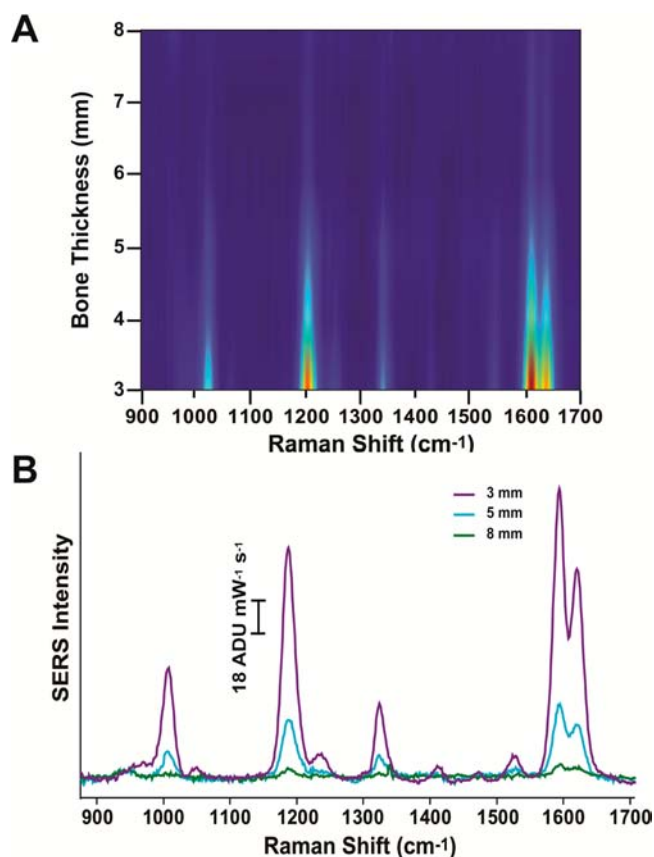
Figure 2. (A) Waterfall plot of baselined SESOR spectra taken at various bone thickness. The false color represents signal intensity from highest (red) to lowest (light blue). (B) Representative baselined SESOR spectra taken at bone thicknesses of 3, 5, and 8 mm. For all spectra, $\lambda_{ex} = 785$ nm, $t = 10$ s, $P = 50$ mW.

Figure 3. Calibration and validation data sets of SESORS quantitative measurements of BPE functionalized SERS nanotags through bone. Spectra of the SERS nanotags were collected at 0× (~9 × 10^{13} particles), 10× (~9 × 10^{12} particles), 20× (~4.5 × 10^{12} particles), 30× (~3 × 10^{12} particles), 35× (~2.6 × 10^{12} particles), and 40× (~2 × 10^{12} particles) concentrations. The LS-SVR calibration plot was constructed using 12 SESORS spectra, and the validation plot was constructed using 6 SESORS spectra. RMSEC = 0.00174 and RMSEP = 2.19; $\lambda_{ex} = 785$ nm, $P = 50$ mW, $t_{acq} = 10$ s.

validation algorithm using MATLAB (Math Works, Natick, MA) and LS-SVM lab1.8 toolbox.[33] Calibration models were developed with SESORS spectra and reference concentrations. Of the three SESORS spectra of each sample collected, two were used to build calibration models and one was used to test the prediction ability of models (Figure 3). Several models with different regularization parameters and kernel widths were generated. The LS-SVR calibration model was chosen as the final model based on performance, which was judged by the root-mean-square error of calibration (RMSEC = 0.00174) and root-mean-square error of prediction (RMSEP = 2.193). LS-SVR is a relatively new class of multivariate methods formulated by Vapnik and co-workers.[34,35] LS-SVR addresses nonlinear effects that are commonly present in biological tissue samples which arise from tissue absorption and scattering. The LS-SVR method develops nonlinear regression models capable of quantitative concentration predictions in complicated biological systems with better accuracy as compared to conventional linear calibration methods such as partial least-squares (PLS).

Figure 3 shows the quantitative prediction ability of SESORS through bone. Twelve randomly chosen independent SESORS measurements were used to build the calibration model, and six additional spectra were used to validate the model. The LS-SVR analysis results in a RMSEC of 0.00174 and a RMSEP of 2.19. As shown in Figure 3, with SESORS we were able to demonstrate quantitative detection ability with reasonable accuracy as most of calibration and validation points closely follow the ideal unity line in the plot. The error in the most diluted sample was larger than those of other sample dilutions. This could be improved by increasing the number of data points in the calibration, especially in the low concentration range.

To summarize, we present the first demonstration of utilizing SESORS for detection of a Raman reporter molecule through bone. All of the peaks of the BPE nanotags were visible in spectra acquired through bone of thicknesses from 3 to 8 mm (which is the average thickness of the human skull). We also demonstrated detection of the BPE nanotags at 40× dilution (~2 × 10^{12} particles), which were validated using a LS-SVR model. The LS-SVR data showed remarkable agreement between the calibration and validation data sets. As current chemically selective imaging techniques are not capable of non-invasive *in vivo* sensing in the brain, we believe that SESORS has enormous potential for use as an *in vivo* spectroscopy approach, and in the future, a Raman imaging technique, for studying neurochemicals in the brain.

■ ASSOCIATED CONTENT

S **Supporting Information**
Original, non-baseline-corrected spectra. This material is available free of charge via the Internet at http://pubs.acs.org.

■ AUTHOR INFORMATION

Corresponding Author
*Corresponding Author vanduyne@northwestern.edu
Notes
The authors declare no competing financial interest.

■ ACKNOWLEDGMENTS

■ REFERENCES

(1) Hillman, E. M. C. *J. Biomed. Opt.* **2007**, *12*, 051402.

(2) Raichle, M. E.; Mintun, M. A. *Annu. Rev. Neurosci.* **2006**, *29*, 449.

(3) Keithley, R. B.; Takmakov, P.; Bucher, E. S.; Belle, A. M.; Owesson-White, C. A.; Park, J.; Wightman, R. M. *Anal. Chem.* **2011**, *83*, 3563.

(4) Venton, B. J.; Wightman, R. M. *Synapse* **2007**, *61*, 37.

(5) Wightman, R. M.; Heien, M. L. A. V.; Wassum, K. M.; Sombers, L. A.; Aragona, B. J.; Khan, A. S.; Ariansen, J. L.; Cheer, J. F.; Phillips, P. E. M.; Carelli, R. M. *Eur. J. Neurosci.* **2007**, *26*, 2046.

(6) Zachek, M. K.; Takmakov, P.; Park, J.; Wightman, R. M.; McCarty, G. S. *Biosens. Bioelectron.* **2010**, *25*, 1179.

(7) Hillman, E. M. C.; Amoozegar, C. B.; Wang, T.; McCaslin, A. F. H.; Bouchard, M. B.; Mansfield, J.; Levenson, R. M. *Philos. Trans. R. Soc. A* **2011**, *369*, 4620.

(8) Fenno, L.; Yizhar, O.; Deisseroth, K. *Annu. Rev. Neurosci.* **2011**, *34*, 389.

(9) Svoboda, K.; Yasuda, R. *Neuron* **2006**, *50*, 823.

(10) Liu, G.; Chen, Z. In *Optical Methods and Instrumentation in Brain Imaging and Therapy*; Madsen, S. J., Ed.; Springer: New York: 2013; Vol. 3, p 157.

(11) Jeanmaire, D. L.; Van Duyne, R. P. *J. Electroanal. Chem. Interfacial Electrochem.* **1977**, *84*, 1.

(12) McNay, G.; Eustace, D.; Smith, W. E.; Faulds, K.; Graham, D. *Appl. Spectrosc.* **2011**, *65*, 825.

(13) Sharma, B.; Frontiera, R. R.; Henry, A.-I.; Ringe, E.; Van Duyne, R. P. *Mater. Today (Oxford, U.K.)* **2012**, *15*, 16.

(14) Sonntag, M. D.; Klingsporn, J. M.; Zrimsek, A. B.; Sharma, B.; Ruvuna, L. K.; Van Duyne, R. P. *Chem. Soc. Rev.* **2014**, DOI: 10.1039/c3cs60187k.

(15) Ando, J.; Yano, T.-a.; Fujita, K.; Kawata, S. *Phys. Chem. Chem. Phys.* **2013**, *15*, 13713.

(16) Culha, M.; Cullum, B.; Lavrik, N.; Klutse, C. K. *J. Nanotech.* **2012**, *2012*, 15.

(17) Han, X. X.; Ozaki, Y.; Zhao, B. *Trends Anal. Chem.* **2012**, *38*, 67.

(18) Matousek, P. *Chem. Soc. Rev.* **2007**, *36*, 1292.

(19) Matousek, P.; Clark, I. P.; Draper, E. R. C.; Morris, M. D.; Goodship, A. E.; Everall, N.; Towrie, M.; Finney, W. F.; Parker, A. W. *Appl. Spectrosc.* **2005**, *59*, 393.

(20) Matousek, P.; Stone, N. *Analyst* **2009**, *134*, 1058.

(21) Matousek, P.; Stone, N. *J. Biophoton.* **2013**, *6*, 7.

(22) Stone, N.; Faulds, K.; Graham, D.; Matousek, P. *Anal. Chem.* **2010**, *82*, 3969.

(23) Stone, N.; Kerssens, M.; Lloyd, G. R.; Faulds, K.; Graham, D.; Matousek, P. *Chem. Sci.* **2011**, *2*, 776.

(24) Ma, K.; Yuen, J. M.; Walsh, J. T.; Glucksberg, M. R.; Van Duyne, R. P. *Anal. Chem.* **2011**, *83*, 9146.

(25) Yuen, J. M.; Shah, N. C.; Walsh, J. T., Jr.; Glucksberg, M. R.; Van Duyne, R. P. *Anal. Chem.* **2010**, *82*, 8382.

(26) Kleinman, S. L.; Sharma, B.; Blaber, M. G.; Henry, A.-I.; Valley, N.; Freeman, R. G.; Natan, M. J.; Schatz, G. C.; Van Duyne, R. P. *J. Am. Chem. Soc.* **2013**, *135*, 301.

(27) Wustholz, K. L.; Henry, A. I.; McMahon, J. M.; Freeman, R. G.; Valley, N.; Piotti, M. E.; Natan, M. J.; Schatz, G. C.; Van Duyne, R. P. *J. Am. Chem. Soc.* **2010**, *132*, 10903.

(28) Firbank, M.; Hiraoka, M.; Essenpreis, M.; Delpy, D. T. *Phys. Med. Biol.* **1993**, *38*, 503.

(29) Bashkatov, A. N.; Genina, E. A.; Kochubey, V. I.; Tuchin, V. V. *Proc. SPIE* **2006**, *6163*, 616310.

(30) Mahinda, H. A. M.; Murty, O. P. *J. Forensic Med. Technnol. (Intl. Ed.)* **2009**, *26*, 26.

(31) Awonusi, A.; Morris, M.; Tecklenburg, M. J. *Calcif. Tissue Intl.* **2007**, *81*, 46.

(32) Yang, W.-h.; Hulteen, J.; Schatz, G. C.; Van Duyne, R. P. *J. Chem. Phys.* **1996**, *104*, 4313.

(33) Suykens, J. A. K.; Van Gestel, T.; De Brabanter, J.; De Moor, B.; Vandewalle, J. *Least Squares Support Vector Machines*; World Scientific Publishing Co.: Singapore, 2002.

(34) Cortes, C.; Vapnik, V. *Mach. Learn.* **1995**, *20*, 273.

(35) Vapnik, V. *The Nature of Statistical Learning Theory*, 2nd ed.; Springer-Verlag: New York, 2000.

17293

dx.doi.org/10.1021/ja409378f | *J. Am. Chem. Soc.* 2013, 135, 17290−17293